Heliyon 6 (2020) e04458

Contents lists available at ScienceDirect

Heliyon

journal homepage: www.cell.com/heliyon

Research article

Effects of growth conditions on properties of CBD synthesized ZnO nanorods grown on ultrasonic spray pyrolysis deposited ZnO seed layers

K. Mosalagae *, D.M. Murape, L.M. Lepodise

Botswana International University of Science and Technology, Private Bag 16, Palapye, Botswana

ARTICLE INFO

Keywords:
Materials science
Nanotechnology
Zinc oxide
Chemical bath deposition
Ultrasonic spray pyrolysis
Raman

ABSTRACT

ZnO nanorods were synthesized on a seed layer coated glass substrate using chemical bath deposition (CBD). Prior to growth, a seed layer had been prepared via ultrasonic spray pyrolysis method. The aim was to explore the influence of varying the chemical bath deposition conditions namely: growth time, bath temperature and concentration levels of the precursor on the orientation, structural, optical and vibrational properties of the subsequently grown nanorods. The presence of ZnO nanorods resembling the hexagonal-wurtzite structure having preference of orientation along the c-axis and varying crystallinity under different growth parameters was confirmed by X-ray diffraction (XRD). Scanning Electron Microscopy (SEM) acquired images of uniformly arranged and vertically oriented ZnO nanorods grown at a relatively higher bath temperature of 90 °C and shorter growth period of 2 h. UV/Vis/NIR spectrophotometer measurements revealed an optical transmittance of between 50 – 70 % for the nanorods. Raman spectroscopy results confirmed the presence of Raman active $E_{2(low)}$ and $E_{2(high)}$ modes corresponding to 98 cm^{-1} and 478 cm^{-1} belonging to the hexagonal ZnO phase. This work shows that the orientation, structural, optical and vibrational properties of the grown nanorod structures are controlled via alteration of the growth parameters.

1. Introduction

ZnO is a promising semiconductor material with indications for suitability in microelectronic and optoelectronic systems applications such as photodetectors, gas sensors, solar cells, light emitting diodes and many others [1]. It is characterized by a wide band gap and exciton binding energy of 3.37 eV and 60 meV respectively [2,3]. It is easy to synthesize and tailor make into different nanostructures such as nanobelts, nanowires, nanorings, nanoflowers and nanorods using several methods [4,5]. Of all the many nanostructures, one dimensional (1D) ZnO nanorods promise to be more suitable for photovoltaic cell applications due to their improved electron transportation efficiency enhanced by a large surface area to volume ratio [6,7].

Various techniques commonly categorized under the gas and solution phase methods have been reported for the synthesis of well aligned 1D ZnO nanorods [8]. Gas phase methods such as metal–organic chemical vapor deposition (MOCVD) [9,10], Vapor phase deposition [11,12,13] and pulse laser deposition [14] among others are very effective at yielding ZnO nanorods of high crystallinity. However high temperatures and complicated costly equipment are required. On the other hand, solution phase method such as CBD are more widely utilized as they require no catalysts and use simple equipment at low temperatures. In addition, CBD is suitable for large scale production of uniform growth of ZnO nanorods on a variety of substrates [15].

In this study a two-step process is reported, where the ultrasonic spray pyrolysis method was used for deposition of the seed layer as the first step. The second step involved the growth of ZnO nanorods via chemical bath deposition. The seed layer acts as nucleation sites thereby maximizing the lattice matching of the substrate and nanorods ensuring vertical orientation of grown ZnO nanorods [16]. Various methods have been used for the deposition of the ZnO seed layers which include spray pyrolysis [4,17,18,19], sputtering [20], spin coating [8,21], dip coating [22], successive ionic layer adsorption and reaction (SILAR) [23] among others. Ultrasonic spray pyrolysis is a simple technique offering several advantages which include; low cost, better control of deposition rate and microstructures thickness, moderate deposition temperatures (300–500 °C) and wide coverage of uniform adherent films or nanoparticles [24,25,26,27,28]. Few studies have been published on the use of ultrasonic spray pyrolysis for seed layer depositions necessitating further investigations [28].

* Corresponding author.
E-mail address: koketsomosalagae@gmail.com (K. Mosalagae).

https://doi.org/10.1016/j.heliyon.2020.e04458
Received 25 April 2020; Received in revised form 24 June 2020; Accepted 10 July 2020

The growth mechanism of nanorods using CBD involves two stages, nucleation followed by growth of the particles in a solution. A solution of a mixture of zinc nitrate hexahydrate and hexamethylenetetramine or hexamine in de-ionized water is often used for the growth of ZnO nanorods by CBD. In most cases, hexamethylenetetramine or hexamine is used as a base to act as a pH buffer to control the solution pH to around 6–7 for the supply of hydroxyl (OH^-) ions [29]. Zinc nitrate hexahydrate is responsible for the production of Zn^{2+} ions while the de-ionized water provides O^{2-} ions for the formation of ZnO [30,31]. ZnO with a hexagonal wurtzite structure consists of polar face of the 002 plane and the non-polar faces of 100 and 101 plane. The polar face is responsible for the faster growth of the crystal along the c-axis. This is due to the less thermodynamic stable surface dipoles of the polar faces compared to that of non-polar faces [32]. The zinc hydroxyl ($Zn(OH)_2$) and (hydroxyl (OH^-) ions are adsorbed by the polar faces as building blocks during the growth process [4]. The effects of chemical bath deposition parameters such as solution concentration, reaction time and temperature on the orientation, shape and size of ZnO nanorods have been extensively studied [4]. However, most studies focused on one parameter instead of investigating various deposition parameters [20]. In this study the influence of several chemical bath deposition parameters, namely precursor concentration, bath temperature and growth time on the morphology, structural, optical and vibrational properties of ZnO nanorods is reported.

2. Experimental details

2.1. Preparation of ZnO seed layer

Ultrasonic spray pyrolysis was used to deposit ZnO seed layers on cleaned glass substrates. The substrates were washed by agitation in acetone, followed by ethanol and de-ionized water for half an hour each in sequence. They were finally blown by nitrogen gas for drying. A solution was then prepared by ultrasonically dissolving 0.15 M of Zinc acetate dihydrate $Zn(CH_3COO)_2).2H_2O$ in 50 ml mixture of ethanol and di-ionized water. The optimized volume ratio of ethanol to di-ionized water used was 1:3 [33]. The prepared solution was then atomized using an ultrasonic nebulizer and delivered to the target substrate by compressed air. The air flow rate and nozzle-substrate distance were maintained at 4.5 L/min and 1.5 cm respectively. The substrate was heated and kept at 400 °C on a hot plate and monitored by a K-type thermocouple. The precursor solution was continuously sprayed on the substrate for 10 min [4,18,34]. After the deposition process, each sample was left to dry on the hot plate for 5 min [4,35]. The samples were then allowed to cool at room temperature. The chemical reactions involved in the deposition of the ZnO seed layers are given by the following equations:

$$Zn(CH_3COO)_2.2H_2O \rightarrow Zn^{2+} + 2CH_3COO^- + 2H_2O \quad (1)$$

$$CH_3COO^- + H_2O \rightarrow CH_3COOH + OH^- \quad (2)$$

$$2OH^- + Zn^{2+} \rightarrow Zn(OH)_2 \quad (3)$$

$$Zn(OH)_2 \rightarrow ZnO + H_2O \quad (4)$$

2.2. Growth of ZnO nanorods

A solution for growing ZnO nanorods was made by mixing equal molar concentrations of zinc nitrate hexahydrate ($Zn(NO_3)_2.6H_2O$) and hexamethylenetetramine (HMTA, $C_6H_{12}N_4$). The two chemicals were dissolved in 100 ml volume of di-ionized water under stirring. Zinc nitrate hexahydrate is responsible for supplying Zn^{2+} for the formation of ZnO nanorods. HMTA hydrolyses in water yielding formaldehyde (HCHO) and ammonia (NH_3). NH_3 then dissolves in water (H_2O) resulting in ammonium (NH^+_4) and hydroxyl (OH^-) ions. OH^- reacts with Zn^{2+} producing Zinc hydroxide $Zn(OH)_2$. Finally, the $Zn(OH)_2$ decomposes into ZnO and water. The chemical reactions leading to a product of ZnO nanorod are given by Eqs. (5), (6), (7), (8), and (9) [36, 37].

$$Zn(NO_3)_2.6H_2O \rightarrow Zn^{2+} + 2NO^-_3 + 6H_2O \quad (5)$$

$$C_6H_{12}N_4 + 6H_2O \rightarrow 6HCHO + 4NH_3 \quad (6)$$

$$NH_3 + H_2O \rightarrow NH^+_4 + OH^- \quad (7)$$

$$2OH^- + Zn^{2+} \rightarrow Zn(OH)_2 \quad (8)$$

$$Zn(OH)_2 \rightarrow ZnO + H_2O \quad (9)$$

The seeded substrates are then vertically suspended in the prepared solution kept at a specific temperature for a certain time. Solution temperatures were increased from 60 °C to 90 °C while the solution concentration was varied from 10 mM to 30 mM. The growth of nanorods was done in times ranging from 1.5 h to 3.0 h. The samples were then rinsed with di-ionized water and blown dry using nitrogen gas. Subsequently, a hot plate was used to anneal all the samples at 400 °C for 60 min. Annealing the samples improves the crystallinity, minimize structural defects and remove organic ligands resulting from the growth solution [38,39,40].

3. Characterization

KLA Tencor D-100 Surface profiler was used to measure the thickness of the ZnO seed layer. The structure and orientation of the ZnO nanorods was revealed by X-ray diffractometer (XRD, D8 Advance, Bruker, Germany). Surface morphologies of the nanostructures were investigated using field emission scanning electron microscopy (FE-SEM, JEOL JSM-7100F). A Varian Cary 500 Scan UV/Vis/NIR Spectrophotometer was used to study the optical transmittance of the ZnO nanorods. Raman spectroscopy studies were done using Horiba-Jobin Yvon Raman Spectrometer (Lab RAM HR Evolution).

4. Results and discussions

4.1. ZnO seed layer morphology

SEM micrograph depicting the surface morphology of ZnO seed layer deposited by ultrasonic spray pyrolysis for 10 min is presented in Figure 1. The SEM image show spherically shaped particles with uniform size, compactness and density. The particles are clustered together and

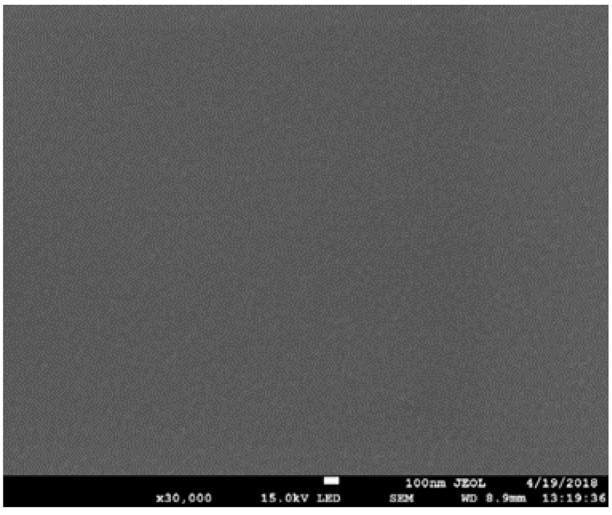

Figure 1. Top-view SEM image of ZnO seed layer deposited by ultrasonic spray pyrolysis.

uniformly distributed suggesting that the nucleation was homogeneous during the seed layer deposition across the substrate. The seed layer thickness measured by KLA Tencor D-100 Surface profiler was found to be approximately 10 nm.

4.2. Growth time effect

Figure 2 shows the top and the cross-sectional appearances (insert) of ZnO nanorods grown from a solution made up of 25 mM concentrations of both Zn $(NO_3)_2.6H_2O$ and HMTA kept at 90 °C while changing the time from 1.5 h to 3.0 h. Statistical distribution of the ZnO nanorods size was determined by randomly measuring from the captured SEM images. Histograms of nanorods diameter distribution with variation of growth time appear as insets in Figure 2. It was observed that the statistics of the nanorods diameter is affected by the growth time. A marginal increase of the average diameter of the nanorods was noted ranging from 60 nm - 80 nm. It was also seen that increasing the growth time from 1.5 h to 3.0 h resulted in an increase in the nanorods average length from 500 nm for 1.5 h to 800 nm for 3 h. This is an indication of a rise in the length to diameter ratio of the nanorods. The axial growth was preferred more as compared to the lateral growth when the growth time was increased as observed from other studies [20,41,42,43].

Long growth periods have been noticed to cause predominant growth along the c-axis of the polar direction (001) as compared to the non-polar faces [31,42]. Most of the ZnO nanorods appear to get tilted as their lengths increase with growth time hence affecting the vertical alignment. As such shorter growth times are preferred for ZnO nanorods fabrication. The best growth time was 2 h as most nanorods were still vertically arranged with high aspect ratio for this study.

Figure 3 (a) illustrates the XRD diffractograms of ZnO nanorods grown for 1.5 h–3 h at 90 °C. The nanorods revealed a wurtzite structured ZnO with the 002 peaks at $2\theta = 34.41^{\circ}$ being dominant indicating the preferred growth along the c-axis. The 002-peak intensified as the growth time changed from 1.5 to 3 h suggesting an improvement in the crystallinity of the nanorods. Similar behaviour was observed in other studies [44,45,46]. Additional weak diffraction peaks for (100) (101) (102) and (103) are observed at 31.76°, 36.25°, 47.57° and 62.96° corresponding to the hexagonal ZnO phase. The presence of the additional peaks indicate the presence of randomly oriented nanorods [47]. All the peaks detected were matching with the standard bulk ZnO (COD 10 11 258) patterns. The mean crystalline sizes (D), strain (ε) and stress (σ) of ZnO nanorods were calculated using the following formulas [48,49,50,51]:

$$D = \frac{0.9\lambda}{\beta cos\theta} \tag{10}$$

$$\varepsilon_{zz} = \frac{c - c_o}{c_o} \tag{11}$$

$$\sigma = -232.8\frac{c - c_o}{c_o} \tag{12}$$

where θ is Bragg's diffraction angle, β is Full Width at Half Maximum (FWHM), λ is the X-ray wavelength (1.5418 Å), c is the lattice parameter of the strained ZnO from the XRD and c_o is the lattice parameter of the unstrained bulk ZnO (COD 10 11 258).

Figure 3 (b) shows a plot of the variation of the FWHM and crystallite sizes as the growth time was varied from 1.5 h to 3.0 h. The FWHM value decreased while the crystallite size increased indicating crystallinity improvement. The strain equation indicates that when the stress is positive, then the sample is under tensile stress, and when the stress is negative then the sample is under compressive stress [52]. Tensile strain of the nanorods gradually decreased with increased growth time from 1.5 h to 3.0 h. The ZnO nanorods also had compressive stress reducing with growth time. Similar trends of stress and strain with growth duration

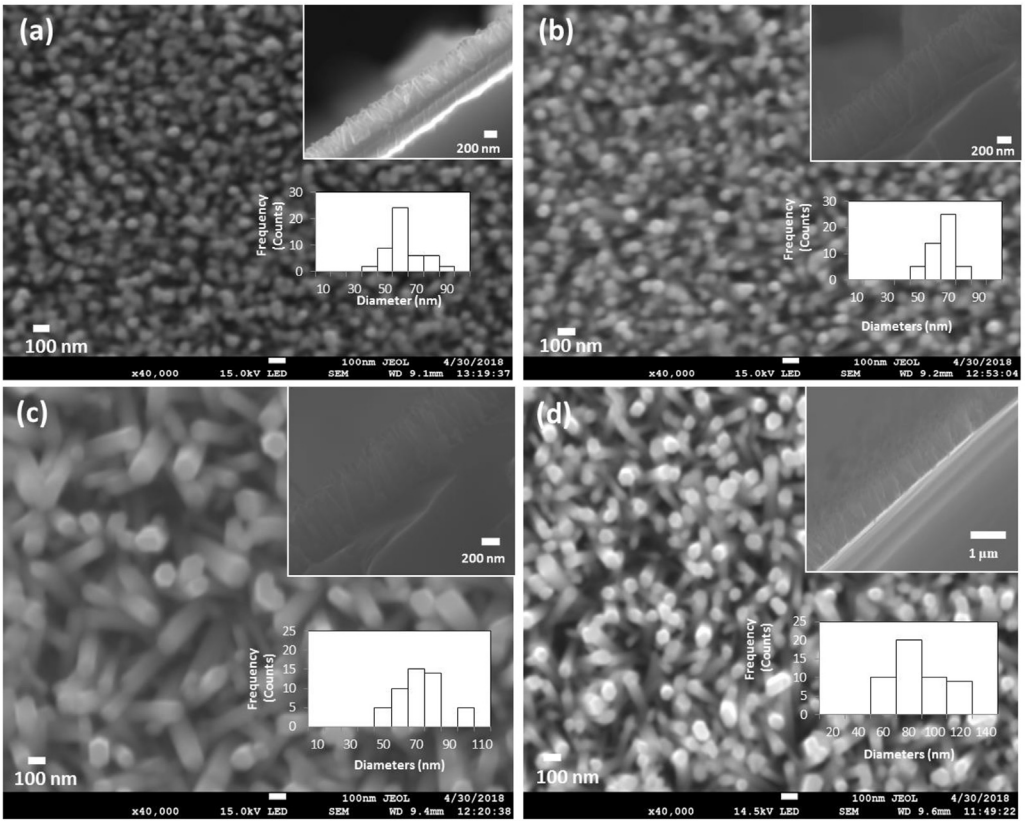

Figure 2. Top-view and cross-sectional view (insert) SEM images of ZnO nanorods grown for (a) 1.5 h; (b) 2h; (c) 2.5 h; (d) 3.0 h. The insert of the histograms in each image correspond to the diameter distribution of the grown nanorods.

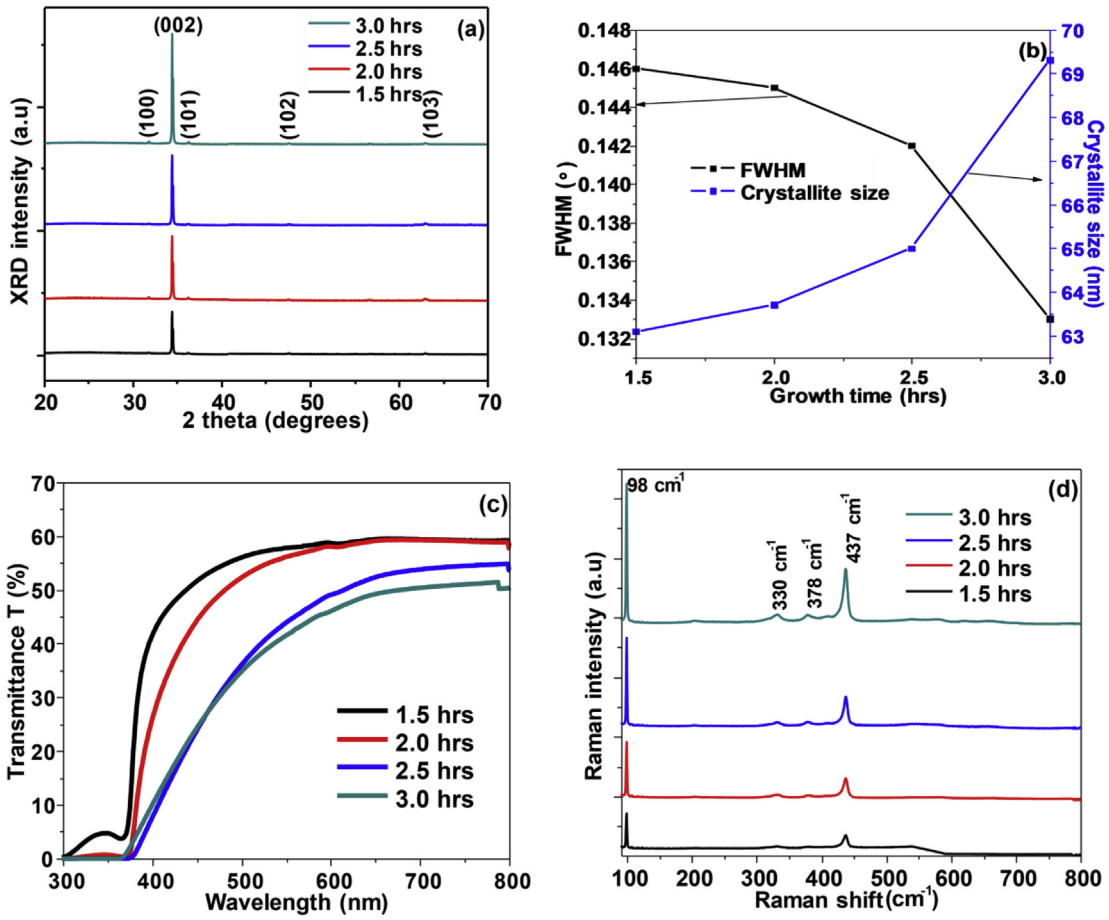

Figure 3. (a) XRD diffractograms; (b) FWHM and crystallite size graph; (c) Optical transmittance spectra; (d) Raman spectra of ZnO nanorods fabricated for 1.5 h–3.0 h.

were observed from other studies [53,54]. Optical transmittance spectra of ZnO nanorods fabricated under variation of growth time from 1.5 h to 3 h are shown in Figure 3 (c). An average of 50–60 % light transmittance was revealed by the nanorods within the visible range. For all the samples the absorption band edges were noticed at around 370–380 nm. The transmittance of the nanorods decreased as the growth time increased. This might have been contributed by increased light scattering effect of the long tilted ZnO nanorods with prolonged growth periods. The transmittance for wavelengths ranging about 300–380 nm for the 1.5 h growth run appears to suggest that nanorods grown for shorter times are not very well networked. The optical band gaps of the nanorods were estimated using the wavelength of the peak corresponding to the absorption band edge obtained from the derivative plot using the following equation:

$$E_g = \frac{hc}{\lambda} \tag{13}$$

where E_g is the band gap energy, h is planks constant (6.626×10^{-34} J s), c is the speed of light (3.0×10^8 m/s) and λ is the wavelength (m) of the peak corresponding to the absorption edge. The band gap energies of the ZnO nanorods as the growth time was varied are listed in Table 1. The values are lower than the 3.37 eV of the standard bulk ZnO. This is mainly due to optical confinement effect of the ZnO nanorods [55]. The band gap energies decreased as the growth time increased from 1.5 to 3 h [56,57]. Crystallite size, stress, strain, oxygen vacancies and carrier concentration are factors that affect the optical band gap energy [58]. From the XRD results obtained the increasing crystallite size, negative stress and positive strain of the nanorods as growth time increased lead to a decrease of the band gap energy.

Figure 3 (d) shows Raman patterns of nanorods grown from a bath solution at 90 °C for 1.5 h–3 h. In the case of wurtzite structured ZnO with two formula units per primitive cell, 8 phonon modes are present. According to the group theory, the phonon modes observable at the Γ point of the Brillouin zone are [59]:

Table 1. Variation of the length, diameter, structural parameters and optical band gap of the nanorods as the growth time increases.

Growth time (*hrs*)	Average length of the nanorods (*nm*)	Average diameter of the nanorods (*nm*)	Crystalline size (nm)	Strain, ε (%) x 10-3	Stress, σ (GPa)	Optical band gap (*eV*)
1.5	400 ± 27	60 ± 12	63.1	0.977	-0.228	3.30
2.0	690 ± 45	67 ± 10	63.7	0.900	-0.210	3.28
2.5	710 ± 47	70 ± 11	65.0	0.888	-0.207	3.25
3.0	800 ± 59	80 ± 23	69.3	0.635	-0.148	3.25

$$\Gamma = 1A_1 + 2B_1 + 1E_1 + 2E_2 \quad (14)$$

Among these modes, $A_1$and E_1 are both Raman and infrared active while $2E_2$ modes are only Raman active. and The $2B_1$ are silent modes. Both the A_1 and E_1 modes divide into longitudinal optical (LO) and transverse optical (TO) phonons [59,60]. A_1 (TO), E_1 (TO), A_1 (LO) and E_1 (LO) modes are related to the impurities and defects such as dopants, Zn interstitials and Oxygen vacancies or their complexes. $2E_2$ modes branch into low and high frequencies. The high frequency modes (E_2 (high)) are associated with the vibration of oxygen atoms while the low frequency modes (E_2 (low)) are related to the vibration of the Zn sublattice. The E_2 modes are non-polar because the ions in each sublattice move in opposite directions leading to zero net polarization [61].

All the nanorods showed Raman peaks at 98 cm^{-1}, 330 cm^{-1}, 378 cm^{-1} and 437 cm^{-1} corresponding to wurtzite structured ZnO. The intensity of the peaks increased with variation of growth time confirming improvement of the crystallinity of the nanorods corroborating with results obtained from the XRD studies. The dominant peaks seen at 98 cm^{-1} and 437 cm^{-1} corresponds to the Raman active E_2 (low) and E_2 (high) modes belonging to ZnO respectively. Additional weak peaks were noticed at 330 cm^{-1} and 378 cm^{-1} associated with combined phonon mode of E_2 (high)- E_2 (low) and A_1 (TO) respectively characteristic to wurtzite ZnO. The peaks observed from all the samples red shifted by 1 cm^{-1} to lower frequencies. The high intensity peak of E_2 (high) is sensitive to the strain hence it is mostly used for analysis. The Raman shifting of the E_2 (high) suggests that the nanorods are under tensile strain concurring with the XRD analysis results.

4.3. Solution temperature effect

Figure 4 shows SEM images of ZnO nanorods grown with variation of solution temperature from 60 °C to 90 °C for 2 h. The compactness and aspect ratios of the nanorods tend to vary as the bath temperature increased from 60 °C to 90 °C. As the temperature increased, the compactness of the nanorods decreased due to faster axial growth rate at higher temperatures. The variation of the average length and diameter of the nanorods were recorded in Table 2. The histograms (insert) of nanorods diameter distribution are also shown in Figure 4. It was noted that the nanorods diameter distribution ranged between 100 nm and 190 nm with temperature variation. The average diameter of the grown nanorods increased from 129 nm to 143 nm as the temperature increased. On the other hand, the length increased from 400 nm to 700 nm as the temperature increased. It was also confirmed that indeed at temperatures as low as 60 °C, the growth of ZnO nanorods by CBD occurs. This agrees with the previous studies [6,62,63,64]. At higher temperatures, the axial growth is favored more than the lateral growth due to improved reaction kinetics leading to fast precipitation of ZnO hence an increase in the length to diameter ratio of the nanorods [65]. As such, the optimum bath temperature for the growth of nanorods was found to be 90 °C.

Figure 5 (a) shows XRD patterns of ZnO nanorods grown for 2 h at 60 °C–90 °C. The XRD diffractograms of all the samples was noticed to be having a dominant peak of 002 plane at $2\theta = 34.4°$ belonging to the hexagonal structured ZnO. The 002 peak intensity increased as the bath temperature was increased from 60 °C to 90 °C indicative of the enhancement of the crystallinity of the nanorods. The present weak peaks of 103 plane at 62.9° seen as the temperature increased belongs to the

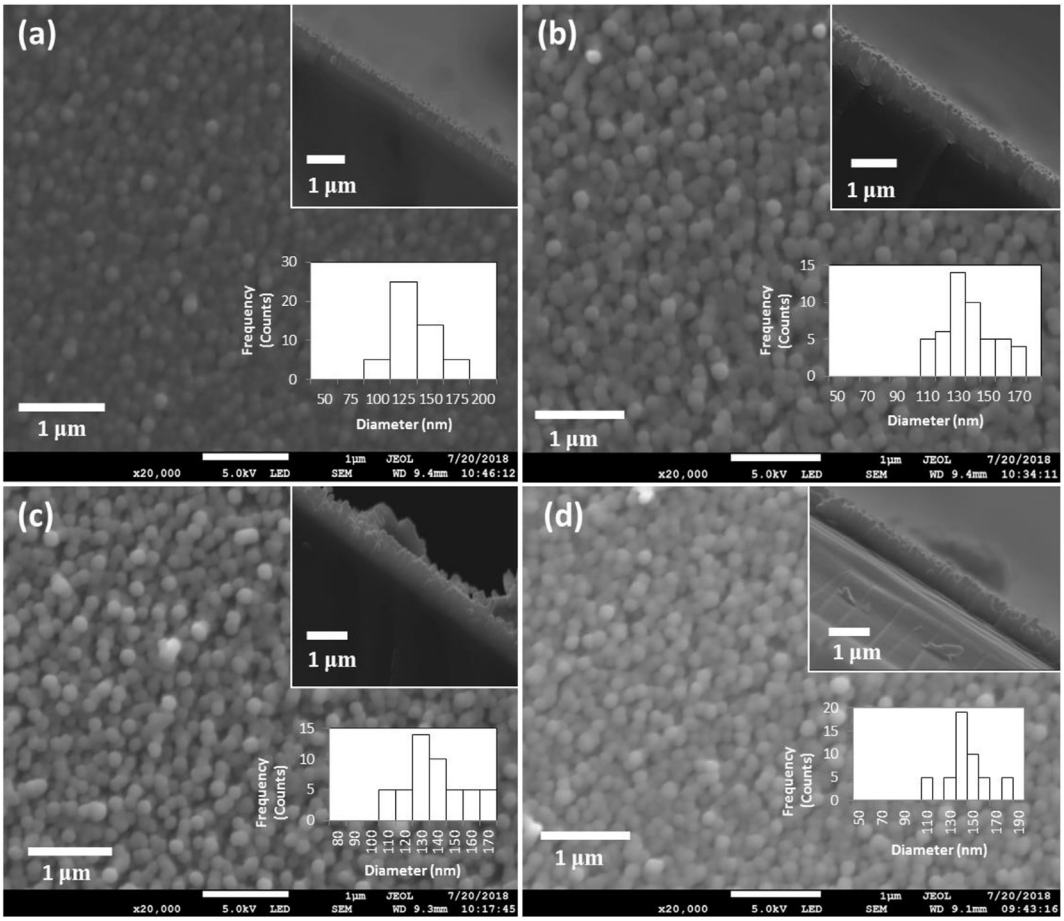

Figure 4. Top-view and cross-sectional view (insert) SEM images of ZnO nanorods grown at (a) 60 °C; (b) 70 °C; (c) 80 °C; (d) 90 °C. Histogram inserts in each SEM image represent nanorods diameter distribution.

Table 2. Variation of the length, diameter, structural parameters and optical band gaps of the grown ZnO nanorods at different temperatures.

Growth Temperature (°C)	Average length of the nanorods (*nm*)	Average diameter of the nanorods (*nm*)	Crystalline size (nm)	Strain, ε (%) x 10^{-3}	Stress, σ (GPa)	Optical band gap (*eV*)
60	400 ± 26	129 ± 17	61.3	1.465	-0.341	3.30
70	657 ± 50	135 ± 20	65.3	1.542	-0.359	3.29
80	671 ± 51	135 ± 20	65.5	1.573	-0.366	3.29
90	700 ± 64	143 ± 25	67.5	1.615	-0.376	3.29

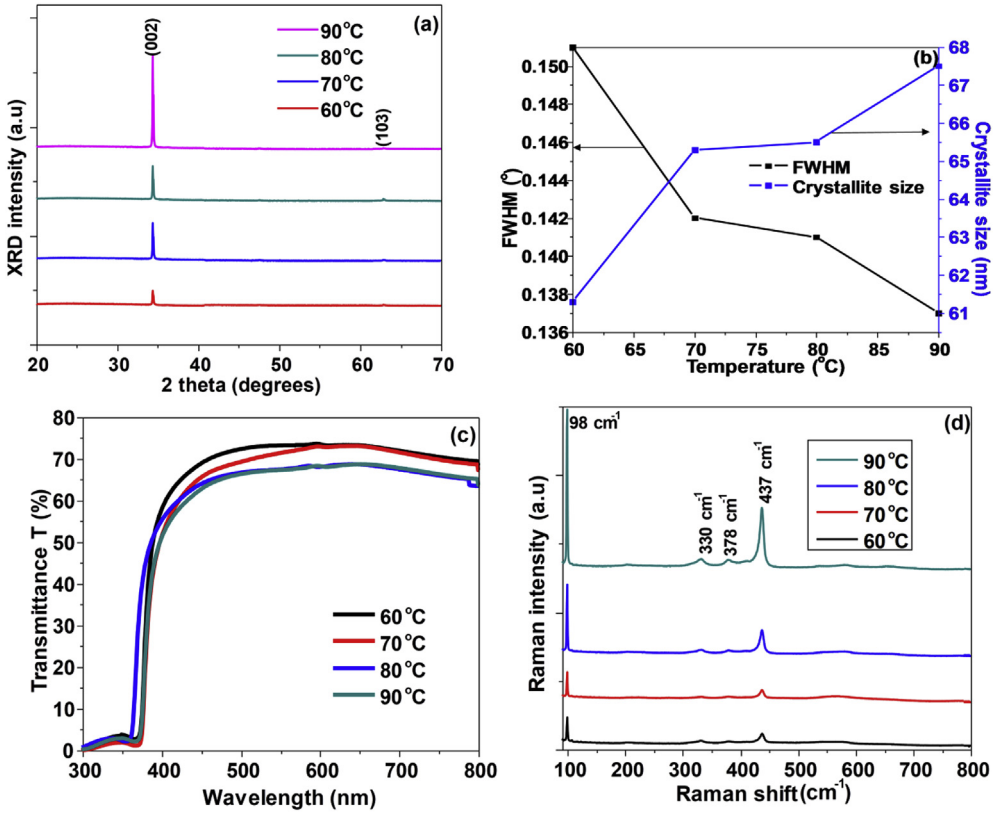

Figure 5. (a) XRD diffractograms; (b) FWHM and crystalline size graph; (c) Optical transmittance spectra; (d) Raman spectra of ZnO nanorods fabricated at 60 °C–90 °C.

ZnO. All the peaks revealed by the XRD are characteristic to hexagonal wurtzite ZnO and agree with pure bulk ZnO pattern (COD 10 11 258). The trend of the crystallite size and FWHM value calculated from Eq. (6) using the 002 peak as the solution temperature varied from 60 °C to 90 °C is shown in Figure 5 (b). The crystalline size increases with a decrease of the FWHM suggesting enhanced crystallinity as the bath temperature increased. The strain on the nanorods was considered using Eq. (11). The positive values obtained suggests that the nanorods are under tensile strain. Eq. (12) was used to determine the stress possessed by the nanorods. The nanorods were under compressive stress as the values found were negative. Both values of strain and stress along the c-axis increased as the temperature increases.

Figure 5 (c) shows optical transmittance spectra of ZnO nanorods prepared while varying growth temperature 60 °C–90 °C. An optical transmittance of 65–75 % was shown by the nanorods in the visible range. The absorption edges were found at around 378 nm. Light transmittance by the nanorods declined as the growth temperature was varied from 60 °C to 90 °C. This is probably due to the increase in the length of the nanorods resulting in enhanced light scattering effect. The values of the band gaps were obtained using the maximum wavelength from the derivative plot and were presented in Table 2. The values slightly decreased from 3.30 eV to 3.29 eV as the temperature increased from 60 °C to 70 °C, and remained constant as temperature was increased to 90 °C. The band gap values exhibit a red shift relative to 3.37 eV of bulk ZnO related to the quantum confinement effect of the synthesized nanorods [55]. A similar trend was observed from other studies [66]. Contrary to our results, the band gap energy obtained from absorbance spectra increased as the temperature increased from 70 °C to 90 °C due to quantum confinement effect [67].

Figure 5 (d) shows Raman patterns of ZnO nanorods fabricated for 2 h at different bath temperatures. Raman peaks detected at 98 cm^{-1}, 330 cm^{-1}, 378 cm^{-1} and 437 cm^{-1} belong to wurtzite structured ZnO. The dominant peaks observed at 98 cm^{-1} and 438 cm^{-1} correspond to the Raman active E_2 (low) and E_2 (high) modes respectively belonging to ZnO. Additional weak peaks were seen at 331 cm^{-1} and 379 cm^{-1} associated with combined phonon mode of E_2 (high)- E_2 (low) and A_1 (TO) respectively, all presenting wurtzite structured ZnO. The peak strength intensified as the growth time increased confirming improvement of the crystallinity of the nanorods corroborating with the XRD results. On the other hand, it is also noted that the position of the peaks from all the samples shifted to lower frequency values when compared to the standard ZnO Raman spectrum. According to other studies, E_2 (high) peak shift arise due to strain [68,69]. The red shifting of the Raman peaks indicates that the nanorods are under the tensile strain in agreement with the XRD data analysis.

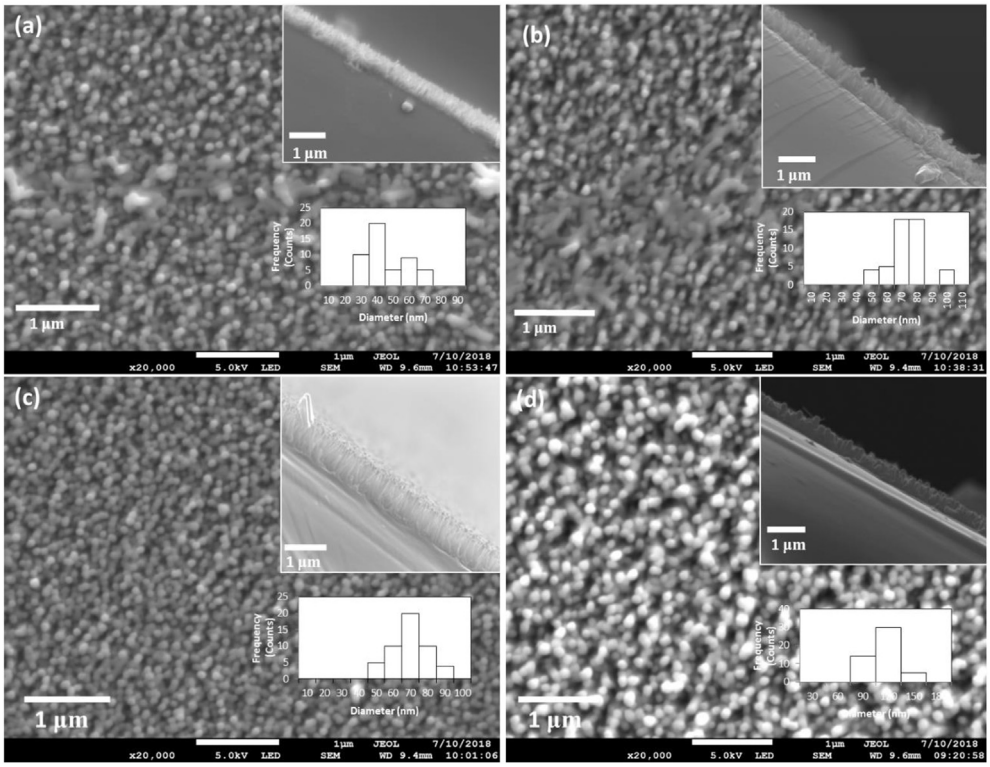

Figure 6. Top-view and cross-sectional view (insert) SEM images and diameter distribution histogram (insert) of ZnO nanorods fabricated from solutions of (a) 10 mM; (b) 15 mM; (c) 25 mM; (d) 30 mM of Zn $(NO_3)_2.6H_2O$ and HMTA.

Table 3. Length, diameter, structural parameters and optical band gap of the nanorods with variation of concentration.

Concentration (mM)	Average length of the nanorods (nm)	Average diameter of the nanorods (nm)	Crystalline size (nm)	Strain, ε (%) X 10-3	Stress, σ (GPa)	Optical band gap (eV)
10	519 ± 46	43 ± 10	59.6	1.019	-0.237	3.31
15	521 ± 47	70 ± 19	61.5	1.335	-0.311	3.31
25	609 ± 51	72 ± 21	64.5	1.412	-0.329	3.30
30	425 ± 25	101 ± 9	65.2	1.715	-0.340	3.29

4.4. Solution concentration effect

Figure 6 shows SEM images of ZnO nanorods grown from variation of solution concentrations of Zn $(NO_3)_2.6H_2O$ and HMTA with temperature kept at 90 °C for 2 h. The length and diameter of the nanorods changed as the concentration of the solutions was varied from 10 mM to 30 mM as indicated in Table 3. Statistical counting of the nanorods diameter distribution was performed from the images and histograms were plotted as shown in Figure 6. The nanorods diameter and distribution is dependent on the concentration as shown in the inserts. The mean diameter continuously increased from 43 nm to 101 nm with variation of solution concentration from 10 mM to 30 mM. On the other hand, as the solution concentration was varied from 10 mM to 25 mM, a significant increase in the average length of the nanorods 519 nm–609 nm was observed. As the concentration increased, the nanorods became thicker due to higher degree of supersaturation. This increase in the mean diameter of the nanorods led to decreased nanorods array density [64]. It was also observed that at lower concentration, the nanorods were disorientated. Similar results were obtained in previous works, observing an increase in the aspect ratio of the nanorods as the concentration increased [62,70,71,72]. The optimum precursor concentration was found to be 25 mM associated with nanorods of high aspect ratio and vertical alignment.

Figure 7 (a) shows XRD patterns of ZnO nanorods fabricated at 90 °C for 2 h while varying growth solution concentrations. The XRD revealed peaks belonging to ZnO concurring with the standard pattern of bulk ZnO (COD 10 11 258). A high intensity 002 peak at 34.4° was observed from all the samples exhibiting the hexagonal ZnO phase. The intensity of the peak improved as the concentration was changed from 10 mM to 25 mM indicating the enhancement of the crystallinity of the grown nanorods. This is due to the polar face of the 002 plane with a faster growth rate than other faces [32]. There is consistency with the SEM results where most vertically aligned nanorods were observed from solution concentrations of 10 mM–25 mM. However, a slight decrease of the peak intensity was observed with further increment of concentration to 30mM as a result of the low nanorods array density. Additional weak peaks of the 100, 101, 102 and 103 planes at 31.7°, 36.2°, 47.5° and 62.9° were also observed from the samples belonging to the ZnO phase. Figure 7 (b) shows plots of the increase in crystalline size and decrease in FWHM as the concentration increased. These indicate crystallinity improvement of the nanorods.

The strain and stress in the nanorods along the c-axis were found using Eqs. (11) and (12) respectively. The values obtained indicated that the nanorods are under tensile strain and compressive stress which may have caused relatively larger c lattice constants. As the concentration increased, both strain and stress of the grown nanorods increased. Figure 7 (c) illustrates the optical transmittance spectra of ZnO nanorods in solutions of various concentrations. All the samples transmitted 60–70 % of the light within the visible range. The absorption band edges were

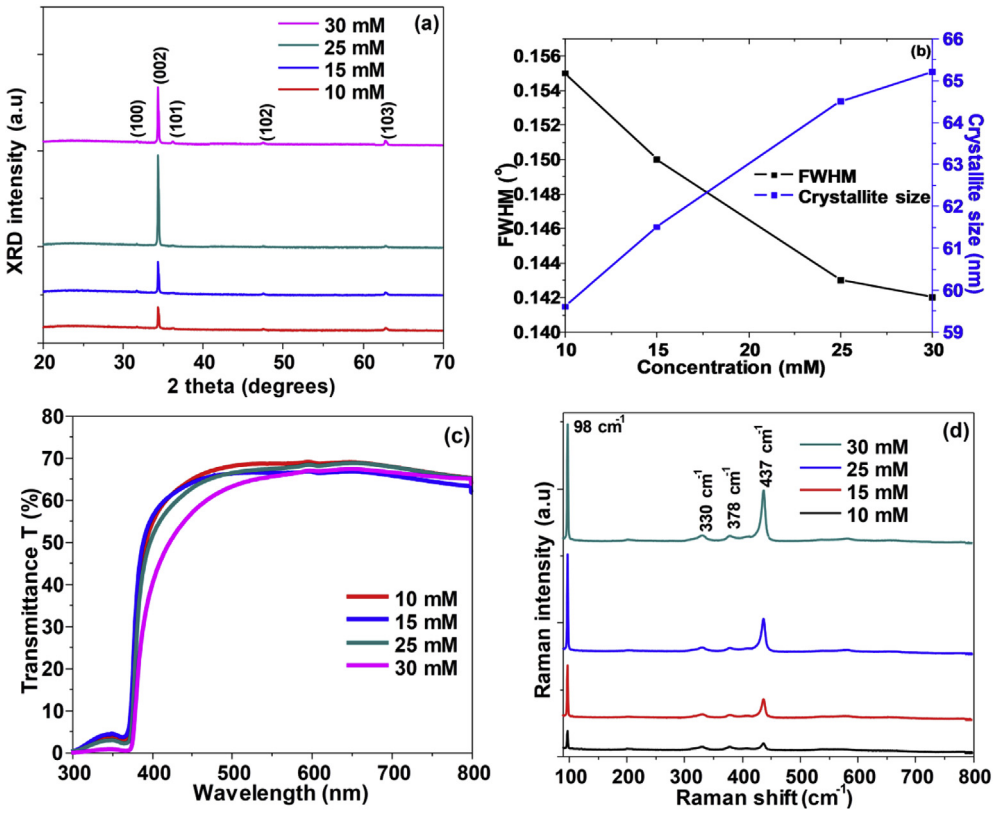

Figure 7. (a) XRD diffractograms; (b) FWHM and crystallite size graph; (c) Optical transmittance spectra; and (d) Raman spectra of ZnO nanorods grown from equal concentration (10mM -30 mM) of zinc nitrate hexahydrate and hexamethylenetetramine.

noticed at around 370nm. The transparency of the nanorods decreased as the precursor concentration varied from 10 mM to 30 mM probably due to the increase in the diameter of the nanorods as shown by the images captured by SEM. The band gap values are slightly lower than the 3.37 eV of the standard bulk ZnO. The band gap values decreased as the concentration was increased as shown in Table 3. The shift of the band gap values from 3.29 eV to 3.31 eV is attributed by stress, strain, oxygen vacancies and carrier concentration [58].

Figure 7 (d) displays Raman spectra of ZnO nanorods grown from variation solutions concentrations. Raman peaks noticed at 98 cm^{-1}, 330 cm^{-1}, 378 cm^{-1} and 437 cm^{-1} belongs to wurtzite structured ZnO. The intensity of the peaks increased as the growth period increased confirming improvement of the crystallinity of the nanorods corroborating with the XRD results. Strong peaks observed at 98 cm^{-1} and 437 cm^{-1} corresponds to the Raman active E_2 (low) and E_2 (high) modes belonging to ZnO respectively. The domination of these modes confirm the good crystallinity of the samples [56,73,74,75]. Weak peaks associated with combined phonon mode of E_2 (high)- E_2 (low) and A_1 (TO) were revealed at 330 cm^{-1} and 378 cm^{-1} respectively characteristic to wurtzite ZnO. The position of the peaks red shifted slightly to lower frequencies indicating that the nanostructures are under tensile strain. The Raman results agree with the XRD and UV/Vis data analysis.

5. Conclusion

CBD method was used successfully to grow ZnO nanorods on glass substrates seeded with ZnO nanoparticles prepared by ultrasonic spray pyrolysis. The influence of CBD growth parameters: growth time, temperature and precursor concentration on the nanorods morphology, structural, optical and vibrational properties were investigated. The length and diameter of the nanorods were observed to increase as the growth time, temperature and precursor concentration increased. The nanorods revealed wurtzite structure of ZnO with a dominant 002 peak. The dominant peaks observed at 98 cm^{-1} and 437 cm^{-1} representing the Raman active E_2 (low) and E_2 (high) modes belonging to ZnO with wurtzite structure respectively were observed from the Raman spectra. The nanorods transmitted 60–70 % of light within the visible range. The optimum growth conditions were; a precursor concentration of 25 mM, temperature of 90 °C and growth time of 2 h characterized with nanorods of high aspect ratio and vertical alignment. The controllability of the properties of ZnO nanorods by variation of growth parameters allow their application in photovoltaic cells as electron transporters.

Declarations

Author contribution statement

K. Mosalagae: Conceived and designed the experiments; Performed the experiments; Analyzed and interpreted the data; Wrote the paper.

D. M. Murape, L. M. Lepodise: Analyzed and interpreted the data; Contributed reagents, materials, analysis tools or data; Wrote the paper.

Funding statement

This research did not receive any specific grant from funding agencies in the public, commercial, or not-for-profit sectors.

Competing interest statement

The authors declare no conflict of interest.

Additional information

No additional information is available for this paper.

Acknowledgements

Special thanks to the Department of Physics and Astronomy, Botswana International University of Science and Technology, Palapye, Botswana for funding the project under Research Grant number: S00028.

References

[1] S. Xu, Z.L. Wang, One-dimensional ZnO nanostructures: solution growth and functional properties, Nano Research 4 (11) (2011) 1013–1098.
[2] V. Srikant, D.R. Clarke, On the optical band gap of zinc oxide, J. Appl. Phys. 83 (10) (1998) 5447.
[3] R. Ayouchi, F. Martin, D. Leinen, J.R. Barrado, Growth of pure ZnO thin films prepared by chemical spray pyrolysis on silicon, J. Cryst. Growth 247 (3-4) (2003) 497–504.
[4] M.A. Mahmood, J. Dutta, Spray pyrolized pre-coating layers for controlled growth of zinc oxide nanorods by hdrothermal pocess, Nanosci. Nanotechnol. - Asia 1 (2) (2011) 92–96.
[5] K.P. Vasudevan, M. Venkatachalam, M. Saroja, P. Gowthaman, S. Shankar, Structural, morphological and optical properties of ZnO nanorods, International Journal of TechnoChem Research 3 (1) (2017) 192–197.
[6] C. Chevalier-César, M. Capochichi-Gnambodoe, Y. Leprince-Wang, Growth mechanism studies of ZnO nanowire arrays via hydrothermal method, Appl. Phys. A 115 (3) (2014) 953–960.
[7] R. Bahramian, A. Moshaii, H. Eshghi, Effect of seeding modification of substrate on the growth and UV detection properties of ZnO nanowires, Mater. Lett. 179 (2016) 222–225.
[8] Z.N. Urgessa, O.S. Oluwafemi, E.J. Olivier, J.H. Neethling, J.R. Botha, Synthesis of well-aligned ZnO nanorods on silicon substrate at lower temperature, J. Alloys Compd. 580 (2013) 120–124.
[9] T. Steiner, Semiconductor Nanostructures for Optoelectronic Applications, Artech Publisher House, Norwood, 2004.
[10] H.O. Pierson, Handbook of Chemical Vapor Deposition - Principles, Technology and Applications, second ed., William Andrew Publishing, New York, 1999.
[11] M. Law, J. Goldberger, P. Yang, Semiconductor nanowires and nanotubes, Annu. Rev. Mater. Res. 34 (2004) 83–122.
[12] A.R. Abramson, W.C. Kim, S.T. Huxtable, H. Yan, Y. Wu, A. Majumdar, C.-L. Tien, P. Yang, Fabrication and characterization of a nanowire/polymer-based nanocomposite for a prototype thermoelectric device, Journal of Microelectromechanical Systems 13 (3) (2004) 505–513.
[13] D.I. Suh, C.C. Byeon, C.L. Lee, Synthesis and optical characterization of vertically grown ZnO nanowires in high crystallinity through vapor–liquid–solid growth mechanism, Appl. Surf. Sci. 257 (5) (2010) 1454–1456.
[14] M.H. Huang, Y. Wu, H. Feick, N. Tran, E. Weber, P. Yang, Catalytic growth of zinc oxide nanowires by vapor transport, Adv. Mater. 13 (2) (2001) 113–116.
[15] S.P. Kumar, M. Yogeshwari, D.A. Raj, D. Mangalaraj, D. Nataraj, U. Pal, Synthesis of vertical ZnO nanorods on glass substrates by simple chemical method, J. Nano Res. 5 (2009) 223–230.
[16] K.H. Kim, K. Utashiro, Y. Abe, M. Kawamura, Growth of zinc oxide nanorods using various seed layer annealing temperatures and substrate materials, International Journal of Electrochemical Science 9 (4) (2014) 2080–2089.
[17] M. Breedon, M.B. Rahmani, S.-H. Keshmiri, W. Wlodarski, K. Kalantar-zadeh, Aqueous synthesis of interconnected ZnO nanowires using spray pyrolysis deposited seed layers, Mater. Lett. 64 (2) (2010) 291–294.
[18] M.F. Ramadhani, M.A.H. Pasaribu, B. Yuliarto, Nugraha, Fabrication of ZnO nanorod using spray-pyrolysis and chemical bath deposition method, AIP Conference Proceedings (2014).
[19] N. Islavath, E. Ramasamy, D. Das, S.V. Joshi, Spray coated seed layer for scalable synthesis of aligned ZnO nanowire arrays on FTO substrate and their photovoltaic properties, Ceram. Int. 41 (3) (2015) 4118–4122.
[20] E. Muchuweni, S.T. Sathiaraj, H. Nyakotyo, Hydrothermal synthesis of ZnO nanowires on rf sputtered Ga and Al co-doped ZnO thin films for solar cell application, J. Alloys Compd. 721 (2017) 45–54.
[21] M. Guo, P. Diao, S. Cai, Hydrothermal growth of well-aligned ZnO nanorod arrays: dependence of morphology and alignment ordering upon preparing conditions, J. Solid State Chem. 178 (6) (2005) 1864–1873.
[22] S. Baruah, J. Dutta, Effect of seeded substrates on hydrothermally grown ZnO nanorods, J. Sol. Gel Sci. Technol. 50 (3) (2009) 456–464.
[23] S. Lindroos, M. Leskela, Growth of zinc peroxide (ZnO2) and zinc oxide (ZnO) thin films by the successive ionic layer adsorption and reaction – SILAR –technique, Int. J. Inorg. Mater. 2 (2-3) (2000) 197–201.
[24] G. Kenanakis, N. Katsarakis, E. Koudoumas, Influence of precursor type, deposition time and doping concentration on the morphological, electrical and optical properties of ZnO and ZnO:Al thin films grown by ultrasonic spray pyrolysis, Thin Solid Films 555 (2014) 62–67.
[25] K. Krunks, O. Bijakina, V. Mikli, T. Varema, E. Mellikov, Zinc Oxide thin films by spray pyrolysis method, Phys. Scripta 79 (1999) 209–212.
[26] E. Muchuweni, T.S. Sathiaraj, H. Nyakotyo, Effect of gallium doping on the structural, optical and electrical properties of zinc oxide thin films prepared by spray pyrolysis, Ceram. Int. 42 (8) (2016) 10066–10070.
[27] P.S. Patil, Versatility of chemical spray pyrolysis technique, Mater. Chem. Phys. 59 (3) (1999) 185–198.
[28] B.A. Rodríguez, Z.L. Peredo, S.M. Rosales, H.J. Torres, G.L. Gonzalez, C.R. Olvera, G.M. Hipólito, G.J. Mendoza, C. Falcony, ZnO nanocolumns synthesized by chemical bath process and spray pyrolysis: ultrasonic and mechanical dispersion of ZnO seeds and their effect on optical and morphological properties, J. Lumin. 218 (2020) 116830.
[29] L.E. Greene, M. Law, J. Goldberger, F. Kim, J.C. Johnson, Y. Zhang, R.J. Saykally, P. Yang, Low-temperature wafer-scale production of ZnO nanowire Arrays, Angew. Chem. Int. Ed. 42 (26) (2003) 3031–3034.
[30] A. Ali, X. Zhao, A. Ali, L. Duan, H. Niu, C. Peng, Y. Wang, S. Hou, Enhanced photocatalytic activity of ZnO nanorods grown on Ga doped seed layer, Superlattice. Microst. 83 (2015) 422–430.
[31] S. Xu, C. Lao, B. Weintraub, Z.L. Wang, Density-controlled growth of aligned ZnO nanowire arrays by seedless chemical approach on smooth surfaces, J. Mater. Res. 23 (8) (2008) 2072–2077.
[32] X. Wu, H. Chen, L. Gong, F. Qu, Y. Zheng, Low temperature growth and properties of ZnO nanorod arrays, Adv. Nat. Sci. Nanosci. Nanotechnol. 2 (3) (2011) 1–4.
[33] J. Rodriguez, F. Paraguay-Delgado, A. Lopez, J. Alarcon, W. Estrada, Synthesis and characterisation of ZnO nanorod films for photocatalytic disinfection of contaminated water, Thin Solid Films 519 (2010) 729–735.
[34] E. Bingöl, M. Tomakin, Investigation of deposition parameters of micro/nanorod ZnO thin films with ultrasonic spray pyrolysis method, Turkish Journal of Materials 2 (2) (2017) 31–37.
[35] N.O. Plank, M.E. Welland, J.L. MacManus-Driscoll, L. Schmidt-Mende, The backing layer dependence of open circuit voltage in ZnO/polymer composite solar cell, Erschienen in: Thin Solid Films 516 (20) (2008) 7218–7222.
[36] X. Yan, Z. Li, R. Chen, W. Gao, Template growth of ZnO nanorods and microrods with controllable densities, Cryst. Growth Des. 8 (7) (2008) 2406–2410.
[37] Q. Li, V. Kumar, Y. Li, H. Zhang, T.J. Marks, R.P.H. Chang, Fabrication of ZnO nanorods and nanotubes in aqueous solutions, Chem. Mater. 17 (5) (2005) 1001–1006.
[38] A. Fernández, J. Fan, A. Cabot, Highly crystalline hydrothermal ZnO nanowires as photoanodes in DSCs, Int. J. Nanotechnol. 11 (9-1011) (2014) 747–757.
[39] J. Fan, Y. Hao, C. Munuera, M. García-Hernández, F. Güell, E.M.J. Johansson, G. Boschloo, A. Hagfeldt, A. Cabot, Influence of the annealing atmosphere on the performance of ZnO nanowire dye-sensitized solar cells, J. Phys. Chem. C 117 (32) (2013) 16349–16356.
[40] J.-L. Wang, T.-Y. Hsieh, P.-Y. Yang, C.-C. Hwang, D.-C. Shye, I.-C. Lee, Oxygen annealing effect on field-emission characteristics of hydrothermally synthesized Al-doped ZnO nanowires, Surf. Coating. Technol. 231 (2013) 423–427.
[41] T.T. Hien, V.A. Minh, B.V. Sang, D.V. Lam, V.N. Hung, N.V. Hieu, N.V. Quy, Facile synthesis of vertically oriented ZnO nanorods for gas sensing application. The 5th International Workshop on Advanced Materials Science and Nanotechnology, IWAMSN2010), Vietnam, 2010.
[42] S. Baruah, J. Dutta, pH-dependent growth of zinc oxide nanorods, J. Cryst. Growth 311 (8) (2009) 2549–2554.
[43] L.Z. Pei, H.S. Zhao, W. Tan, Hydrothermal oxidization preparation of ZnO nanorods on zinc substrate, Phys. E Low-dimens. Syst. Nanostruct. 42 (5) (2010) 1333–1337.
[44] J.Y. Chen, K.W. Sun, Growth of vertically aligned ZnO nanorod arrays as antireflection layer on silicon solar cells, Sol. Energy Mater. Sol. Cell. 94 (5) (2010) 930–934.
[45] T.-h. Lee, H. Ryu, W.-J. Lee, Fast vertical growth of ZnO nanorods using a modified chemical bath deposition, J. Alloys Compd. 597 (2014) 85–90.
[46] M.C. Kao, H.Z. Chen, S.L. Young, C.C. Lin, C.Y. Kung, Structure and photovoltaic properties of ZnO nanowire for dye-sensitized solar cells, Nanoscale Research Letters 7 (2012) 260.
[47] E. Muchuweni, T.S. Sathiaraj, H. Nyakotyo, Effect of annealing on the microstructural, optical and electrical properties of ZnO nanowires by hydrothermal synthesis for transparent electrode fabrication, Mater. Sci. Eng. B 227 (2018) 68–73.
[48] P.R. Deshmukh, Y. Sohn, W.G. Shin, Chemical synthesis of ZnO nanorods: investigations of electrochemical performance and photo-electrochemical water splitting applications, J. Alloys Compd. 711 (2017) 573–580.
[49] D.I. Rusu, G.G. Rusu, D. Luca, Structural characteristics and optical properties of thermally oxidized zinc films, Acta Phys. Pol., A 119 (6) (2011) 850–856.
[50] A. Singh, H.L. Vishwakarma, Study of structural, morphological, optical and electroluminescent properties of undoped ZnO nanorods grown by a simple chemical precipitation, Materials Science-Poland 33 (4) (2015) 751–759.
[51] J. Kennedy, P.P. Murmu, J. Leveneur, A. Markwitz, J. Futter, Controlling preferred orientation and electrical conductivity of zinc oxide thin films by post growth annealing treatment, Appl. Surf. Sci. 367 (2016) 52–58.
[52] E. Karaköse, H. Çolak, Effect of substrate temperature on the structural properties of ZnO nanorods, Energy 141 (2017) 50–55.
[53] R. Shabannia, Vertically aligned ZnO nanorods on porous silicon substrates: effect of growth time, Prog. Nat. Sci.: Materials International 25 (2) (2015) 95–100.
[54] O.F. Farhat, M.M. Halim, N.M. Ahmed, A.A. Oglat, A.A. Abuelsamen, M. Bououdina, M.A. Qaeed, A study of the effects of aligned vertically growth time on ZnO nanorods deposited for the first time on Teflon substrate, Appl. Surf. Sci. 426 (2017) 906–912.
[55] K.L. Foo, U. Hashim, K. Muhammad, C.H. Voon, Sol-gel synthesized zinc oxide nanorods and their structural and optical investigation for optoelectronic application, Nanoscale Research Letters 9 (1) (2014) 1–10.
[56] A.F. Abdulrahman, S.M. Ahmed, M.A. Almessiere, Effect of the growth time on the optical properties of ZnO nanorods grown by low temperature method, Digest Journal of Nanomaterials and Biostructures 12 (4) (2017) 1001–1009.
[57] L.M. Fudzi, Z. Zainal, H.N. Lim, S.-K. Chang, A.M. Holi, M.S. Ali, Effect of temperature and growth time on vertically aligned ZnO nanorods by simplified hydrothermal technique for photoelectrochemical cells, Materials 11 (5) (2018) 1–13.

[58] B.L. Zhu, X.H. Sun, S.S. Guo, X.Z. Zhao, J. Wu, R. Wu, J. Liu, Effect of thickness on the structure and properties of ZnO thin films prepared by pulsed laser deposition, Jpn. J. Appl. Phys. 45 (10A) (2006) 7860–7865.
[59] H. Morkoç, Ü. Özgür, Zinc Oxide: Fundamentals, Materials and Device Technology, WILEY-VCH Verlag GmbH & Co. KGaA, Weinheim, 2008.
[60] H.-C. Hsu, H.-M. Cheng, C.-Y. Wu, H.-S. Huang, Y.-C. Lee, W.-F. Hsieh, Luminescence of selective area growth of epitaxial ZnO nanowires and random-growth-oriented nanobelts, Nanotechnology 17 (5) (2006) 1404–1407.
[61] V. Russo, M. Ghidelli, P. Gondoni, C.S. Casari, A.L. Bassi, Multi-wavelength Raman scattering of nanostructured Al-doped zinc oxide, J. Appl. Phys. 115 (7) (2014) 1–27.
[62] Q. Li, J. Bian, J. Sun, J. Wang, Y. Luo, K. Sun, D. Yu, Controllable growth of well-aligned ZnO nanorod arrays by low-temperature wet chemical bath deposition method, Appl. Surf. Sci. 256 (6) (2010) 1698–1702.
[63] M. Poornajar, P. Marashi, D.H. Fatmehsari, M.K. Esfahani, Synthesis of ZnO nanorods via chemical bath deposition method: the effects of physicochemical factors, Ceram. Int. 42 (1) (2016) 173–184.
[64] J. Yu, Z. Yuan, S. Han, Z. Ma, Size-selected growth of transparent well-aligned ZnO nanowire arrays, Nanoscale Research Letters 7 (517) (2012) 1–6.
[65] Y.E. Kalay, H.E. Unalan, Hydrothermal zinc oxide nanowire growth using zinc acetate salt, J. Mater. Res. 27 (11) (2012) 1445–1451.
[66] N. Mufti, I.K.R. Laila, R. Idiawati, A. Fuad, A. Hidayat, A. Taufiq, Sunaryono, The effect of growth temperature on the characteristics of ZnO nanorods and its optical properties, J. Phys. Conf. 1057 (1) (2018) 1–9.
[67] L. Zhang, Y. Ruan, Y. Liu, Y. Zhai, Effect of growth temperature on the structure and optical properties of ZnO nanorod arrays grown on ITO substrate, Cryst. Res. Technol. 48 (11) (2013) 996–1002.
[68] G.-z. Jia, B.X. Hao, X.C. Lu, X. Wang, Y.M. Li, J.H. Yao, Solution growth of well-aligned ZnO nanorods on sapphire substrate, Acta Physica Polonica Series 124 (1) (2013) 74–77.
[69] O.F. Farhat, M.M. Halim, M.J. Abdullah, M.K.M. Ali, N.K. Allam, Morphological and structural characterization of single-crystal ZnO nanorod arrays on flexible and non-flexible substrates, Beilstein J. Nanotechnol. 6 (2015) 720–725.
[70] J.-J. Dong, C.-Y. Zhen, H.-Y. Hao, J. Xing, Z.-L. Zhang, Z.-Y. Zheng, X.-W. Zhang, Controllable synthesis of ZnO nanostructures on the Si substrate by a hydrothermal route, Nanoscale Research Letters 8 (378) (2013) 1–7.
[71] D. Polsongkram, P. Chamninok, S. Pukird, L. Chow, O. Lupan, G. Chai, H. Khallaf, S. Park, A. Schulte, Effect of synthesis conditions on the growth of ZnO nanorods via hydrothermal method, Physica B 403 (2008) 3713–3717.
[72] G. Amin, M. Asif, A. Zainelabdin, S. Zaman, O. Nour, M. Willander, Influence of pH, precursor concentration, growth time, and temperature on the morphology of ZnO nanostructures grown by the hydrothermal method, J. Nanomater. 2011 (269692) (2011) 1–9.
[73] N.I. Rusli, M. Tanikawa, M.R. Mahmood, K. Yasui, A.M. Hashim, Growth of high-density zinc oxide nanorods on porous silicon by thermal evaporation, Materials 5 (12) (2012) 2817–2832.
[74] V.A. Coleman, C. Jagadish, Zinc oxide bulk, thin films and nanostructures: processing, properties and applications, in: Basic Properties and Applications of ZnO, Elsevier, Oxford, 2006, pp. 1–20.
[75] Q. Zhao, X.Y. Xu, X.F. Song, X.Z. Zhang, D.P. Yu, Enhanced field emission from ZnO nanorods via thermal annealing in oxygen, Appl. Phys. Lett. 88 (3) (2006) 33102–33105.